Langmuir

Article

pubs.acs.org/Langmuir

Capillary Condensation Hysteresis in Overlapping Spherical Pores: A Monte Carlo Simulation Study

Gennady Yu. Gor,[†] Christopher J. Rasmussen, and Alexander V. Neimark*

Department of Chemical and Biochemical Engineering, Rutgers, The State University of New Jersey, 98 Brett Road, Piscataway, New Jersey 08854, United States

ABSTRACT: The mechanisms of hysteretic phase transformations in fluids confined to porous bodies depend on the size and shape of pores, as well as their connectivity. We present a Monte Carlo simulation study of capillary condensation and evaporation cycles in the course of Lennard-Jones fluid adsorption in the system of overlapping spherical pores. This model system mimics pore shape and connectivity in some mesoporous materials obtained by templating cubic surfactant mesophases or colloidal crystals. We show different mechanisms of capillary hysteresis depending on the size of the window between the pores. For the system with a small window, the hysteresis cycle is similar to that in a single spherical pore: capillary condensation takes place upon achieving the limit of stability of adsorption film and evaporation is triggered by cavitation. When the window is large enough, the capillary condensation shifts to a pressure higher than that of the isolated pore, and the possibility for the equilibrium mechanism of desorption is revealed. These finding may have important implications for practical problems of assessment of the pore size distributions in mesoporous materials with cagelike pore networks.

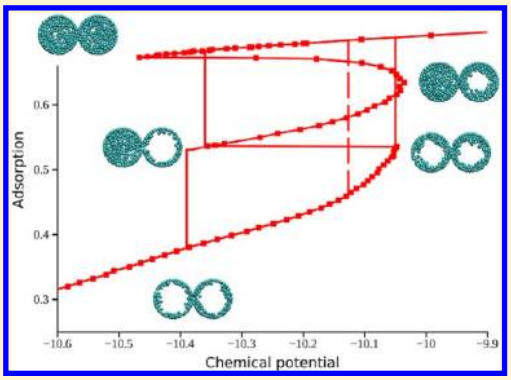

1. INTRODUCTION

Gas adsorption is a standard technique for the characterization of porous materials. Often experimental adsorption isotherms are irreversible, showing adsorption−desorption hysteresis. A proper interpretation of the physical mechanisms of hysteresis is crucial for the assessment of the pore size distributions from adsorption isotherms.[1−4] For a number of materials, predicting hysteresis when modeling adsorption requires taking into account not just the pore geometry but the pore connectivity[5−7] and/or morphological defects.[8,9]

Recent developments in material science[10] enabled the fabrication of mesoporous silicas and carbons with 3D regular and hierarchical pore networks and tunable pore size distributions.[11] Usually, the cagelike wider mesopores are connected by narrower channels; such pores are called "ink-bottle" pores,[12] referring to larger pores as cavities and to smaller connecting channels as necks, as illustrated in Figure 1a. Ink-bottle pores are of interest because of the unique confinement effects observed upon adsorption, depending on the ranges of cavity and neck sizes.[13−15]

While the capillary condensation process upon adsorption in ink-bottle pores is determined by the size of the cavity and takes place near the vapor spinodal of the confined fluid,[16] the desorption (evaporation) process is more complicated. Experimental observations with specially designed ordered materials and respective theoretical analysis[17] revealed three different mechanisms of evaporation from cagelike mesopores: (i) pore-blocking-controlled desorption, (ii) spontaneous evaporation due to cavitation, and (iii) near-equilibrium desorption. The prevalence of a given mechanism and thus the pressure p_d at which desorption occurs depends mainly on the relation between the size of the cavity and the size of the necks.[13−15] Near-equilibrium desorption is possible from the cavities that have immediate access to the vapor phase through relatively wide openings and thus are effectively unblocked. Once the vapor pressure reaches the vapor−liquid equilibrium (VLE) pressure p_e^{cavity}, desorption from the main cavity proceeds via a receding meniscus; therefore, $p_d \approx p_e$. However, if wide cavities are connected with narrower necks so that the fluid in the neck has a lower VLE pressure p_e^{neck} than that of the fluid in the cavity, the neck effectively "blocks" desorption from the cavity. Emptying of the pores occurs at the pressure of equilibrium desorption of the neck, and as such, $p_d = p_e^{neck}$ and becomes a function of the neck size. Finally, if the connecting necks are even narrower, then the fluid in the cavity becomes substantially metastable and the vapor pressure may reach the spinodal point of the confined liquid before the equilibrium meniscus can form in the neck. Thus, the fluid desorbs from the

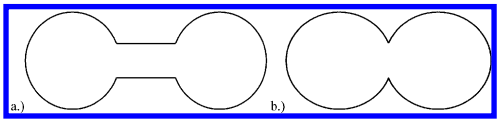

Figure 1. Models of interconnected spherical pores: (a) Classical ink-bottle pore. (b) Overlapping pores, considered in the current work.

Received: June 7, 2012
Revised: July 20, 2012
Published: July 23, 2012

pore by the cavitation mechanism, which involves the fluctuation-driven formation and growth of a bubble.[18] In this scenario, $p_d \ll p_e$ and p_d has little or no dependence on the size of the necks.[14] Available models of pore blocking[19] and cavitation[14] (which represent the pores as spheres connected with cylinders) describe adsorption in materials such as FDU-1[20] or SBA-16[21] silicas reasonably well.

However, there exist mesoporous materials with cagelike pores that likely overlap rather than connect by narrow channels. One such class of materials is the novel 3D-ordered mesoporous (3DOm) carbons,[22] synthesized by templating densely packed spherical nanoparticles. Nitrogen adsorption experiments in 3DOm carbons have revealed the IUPAC H1 type of hysteresis.[16] Although experimental values of capillary condensation pressures are in good agreement with predictions from density functional theory (DFT),[23] the values of capillary evaporation pressures ($p_d/p_0 \approx 0.6–0.7$,where p_0 is the bulk VLE pressure)[22,24] cannot be explained either as homogeneous cavitation or as equilibrium desorption. Other novel materials possessing similar structure and revealing similar capillary condensation hysteresis are ultraporous DVB resins.[25]

To reveal the possible mechanisms of evaporation in such a neckless ink-bottle pore, we modeled a system of two overlapping spheres (Figure 1b). We should emphasize that we do not consider classical ink-bottle pores with connecting channels (necks), depicted in Figure 1a. Adsorption and confinement effects were modeled with Lennard-Jones (LJ) particles using grand canonical Monte Carlo (GCMC)[26] and mesocanonical Monte Carlo (MCMC) simulation techniques.[27,28] The fluid–solid interaction was treated as an integration of the LJ potential over two spherical layers, where the degree of overlap is set before integration. The resulting potential is continuous and depends on the window size. The goal of our simulations is to estimate the influence of the window size on the capillary condensation and evaporation pressures. In the current work, we do not explicitly consider the connection of the pore with an external reservoir but rather consider a closed system of two pores, representing a characteristic element of the pore network. However, such a model is sufficient to reveal the role of the window size.

The structure of the rest of the article is the following. The pore model and MC methods used are described in Section 2. Section 3 presents the results of MC simulations, their comparison to previous models, and a discussion. Conclusions are given in Section 4.

2. MODEL AND SIMULATIONS DETAILS

Monte Carlo simulations were used to model adsorption/desorption in the two-pore model (Figure 1b) with an external pore diameter (the diameter of the sphere as the distance of a line drawn through the centers of solid atoms at opposite pore wall surfaces) of $d_{ext} = 5.72$ nm $= 15.82\sigma_{FF}$ and the internal diameter defined as the distance encompassing two opposite fluid particles whose adsorption potential is zero. For the solid–fluid potential used, $d_{int} = d_{ext} - 1.7168\sigma_{SF} + \sigma_{FF}$, so $d_{int} = 5.54$ nm $= 15.32\sigma_{FF}$. We considered two characteristic values of the window size, $5\sigma_{FF}$ and $10\sigma_{FF}$. The adsorbing fluid was LJ nitrogen, with fluid–fluid interaction parameters of $\varepsilon_{FF}/k_B = 101.5$ K and $\sigma_{FF} = 0.36154$ nm.[29] The potential energy was truncated when the interparticle distance was greater than $5\sigma_{FF}$. A spherically integrated, site-averaged LJ potential was used to model the attractive adsorption potential.[15,30] The solid–fluid interaction parameters were selected to emulate the adsorption of nitrogen on silica (energy parameter $\varepsilon_{SF}/k_B = 147.3$ K, size parameter $\sigma_{SF} = 0.317$ nm, and surface density of adsorption sites $\rho_S = 15.3$ nm^{-2}).[31] For all simulations, the temperature was set to the normal boiling point of liquid nitrogen, $T = 77.36$ K. The dimensions and chemistry of the model system were selected for quantitative comparison to the single-sphere pore model, for which there are published results.[14,32]

The interaction potential between a fluid particle and the substrate was obtained by the superposition of potentials from a sphere with a window. The latter can be obtained by partial integration of the LJ potential over the spherical domain depicted in Figure 2. The interaction potential between a fluid particle and the pore wall at a given point with spherical coordinates (r, θ, φ) is given by equation

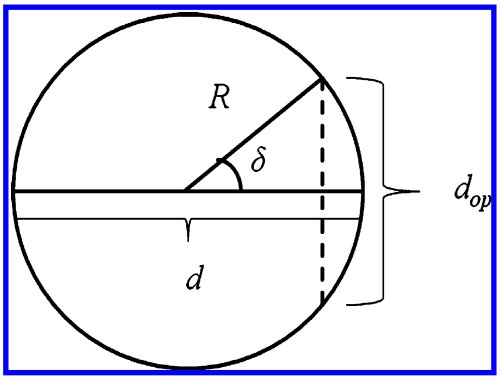

Figure 2. Model of the spherical pore with a window.

$$U_{SF}(r, \theta, \delta, R) = 4\varepsilon_{SF}\rho_S R^2 \int_0^{2\pi}\int_\delta^\pi \left(\frac{\sigma_{SF}^{12}}{\xi^{12}} - \frac{\sigma_{SF}^{6}}{\xi^{6}}\right) \cdot \sin\theta_0 \, d\theta_0 \, d\varphi_0 \quad (1)$$

where δ is size of the polar angle that contributes to the window, R is the external radius of the pore body, and subscript 0 indicates integration variables over the spherical surface. The distance ξ from a given point within the sphere (e.g., an adsorbate molecule) to a point on the surface of the sphere (e.g., an adsorption site) is

$$\xi^2 = R^2 + r^2 - 2Rr[\sin\theta \sin\theta_0 \cos(\varphi_0 - \varphi) + \cos\theta \cos\theta_0] \quad (2)$$

Equation 1 does not depend on the azimuth coordinate φ due to the axial symmetry of the sphere with a round window. A simple trigonometric equation relates δ to the size (diameter) of the window, as shown in Figure 2. The value d_{op} specifies the external (center-to-center) diameter of the circular window between the two spheres. An interaction potential map of the considered systems is displayed in Figure 3. Equation 1 was integrated numerically over 200 bins in the (θ_0, φ_0) coordinates. We found that additional bins did not reduce the integration error. The resulting function was stored in a 2001 × 2001 lookup table, and bilinear interpolation was used to compute the solid–fluid interaction energy for a given particle in cylindrical coordinates (ρ, z).

Monte Carlo simulations were performed in the grand canonical ensemble (GCMC)[26] and the mesocanonical ensemble (MCMC), also known as the gauge cell method.[27,28] The MCMC method is instrumental in calculating chemical

dx.doi.org/10.1021/la302318j | Langmuir 2012, 28, 12100–12107

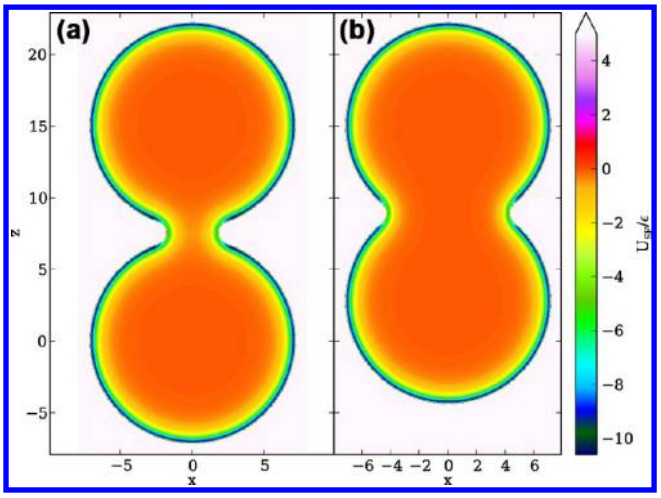

Figure 3. Solid–fluid potential energy map of a system of two spheres of $15.82\sigma_{FF}$ each with (a) a $5\sigma_{FF}$ window and (b) a $10\sigma_{FF}$ window. Both distance and potential are given in LJ units.

potentials in small inhomogeneous systems and in analyzing metastable and labile states inside the hysteresis loop.[33] It has been extended since its original formulation[27] to multicomponent fluids[34] and polymer chains.[35,36] MCMC introduces a fixed reservoir of particles (gauge cell) that is permitted to exchange fluid with the system cell (pore). Use of the gauge cell allows for the efficient calculation of the chemical potential μ at given adsorption N (up to an order of magnitude faster than traditional Widom insertions)[36] as well as suppressing fluctuations that would, if unconstrained, facilitate a phase change in an open system. Therefore, the gauge cell allows for the stabilization in the system cell of metastable and labile states, such as critical nuclei, because the combined system (system cell + gauge cell) is thermodynamically stable. As such, the MCMC simulation enables the generation of a continuous canonical adsorption isotherm $N(\mu)$ of the van der Waals type with a backward trajectory that connects the vapor and liquid spinodals. In doing so, the Helmholtz free energy and, respectively, the work of formation of the critical nuclei that precedes cavitation desorption can be calculated using thermodynamic integration.

GCMC was used to emulate experimental adsorption conditions, that is, constant chemical potential, volume, and temperature in an open system. GCMC in this sense was used to test the stability of a given configuration of particles. The final configuration from an MCMC simulation, which can exist as a stable, metastable, or unstable system, was used as the initial configuration for a GCMC simulation. The chemical potential was set from previous MCMC simulations as well. The stability of a state generated in MCMC can be verified in the GCMC simulation starting with that particular configuration. Labile configurations cannot be stabilized in the open system implied by GCMC.

3. RESULTS AND DISCUSSION

Using GCMC and MCMC simulations, we have studied the adsorption of LJ nitrogen in the two-pore system constructed of overlapping spheres of $15.82\sigma_{FF}$ diameter with two window sizes: $5\sigma_{FF}$ and $10\sigma_{FF}$. Adsorption isotherms for both systems are presented in Figure 4, along with the canonical isotherm obtained from MCMC and the GCMC isotherm for a single spherical pore of the same size from ref 14. Adsorption amounts were normalized as the dimensionless fluid density $\rho = N\sigma_{FF}^3/V$, where V is the total volume of the system calculated with the internal diameter.

Figure 4a demonstrates a qualitative difference between the canonical isotherms for a single spherical pore and a two-pore system. The two-pore system isotherm has an intermediate loop, which is indicative of dissimilar phase behavior in the connected pores. The physical states of the two-pore system corresponding to the characteristic points of the isotherm are revealed by the snapshots in Figure 5. Line AB corresponds to the growth of the film on the pore walls (vaporlike state) and does not differ from the analogous branch of the isotherm for a single pore. At point B, the film reaches the limit of its stability and capillary condensation takes place in one of the pores (point C). Thus, the fluid in one of the pores is in its liquidlike state, and the other remains in the vaporlike state; this is clearly seen in the snapshot for point C in Figure 5. Line CD presents a number of quasi-equilibrium states similar to the one presented by point C. These states do not represent true equilibrium configurations but exist because of the stabilization

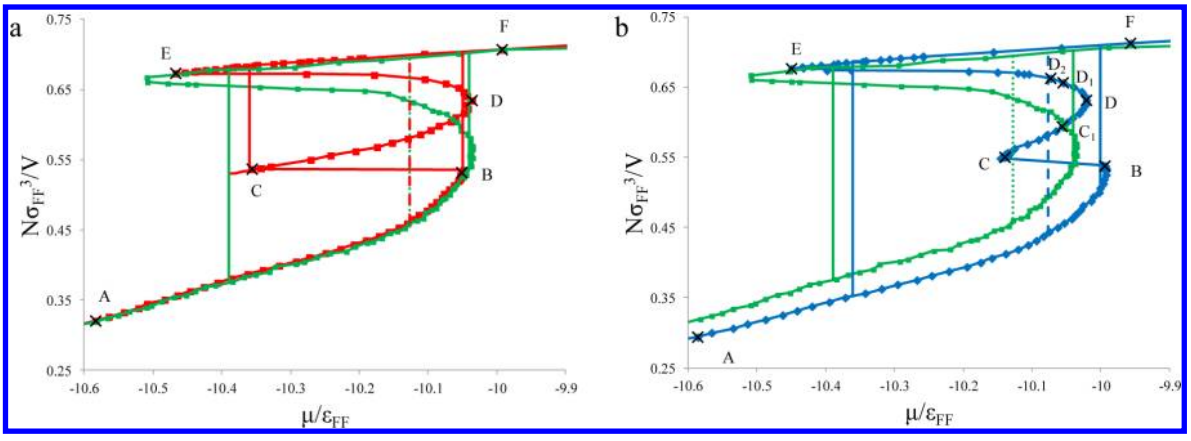

Figure 4. Isotherms calculated by MCMC (lines with markers) and GCMC (solid lines without markers) from simulations in the system with (a) a $5\sigma_{FF}$ window and (b) a $10\sigma_{FF}$ window. Green solid lines in both panels represent the adsorption isotherm for a single spherical pore of the same size from ref 14. One of the desorption steps for the two-pore system in panel (a) coincides with the desorption transition for a single pore. Vertical dashed lines indicate the positions of vapor–liquid equilibrium chemical potentials calculated for each system by applying the Maxwell rule to continuous canonical isotherms.

dx.doi.org/10.1021/la302318j | *Langmuir* 2012, 28, 12100–12107

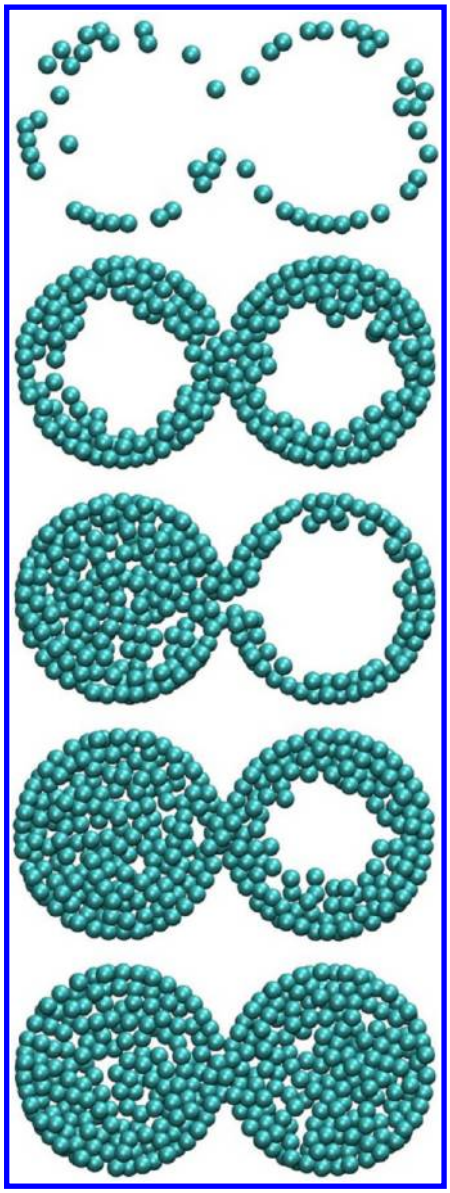

Figure 5. Snapshots of the molecules adsorbing in a system of two spheres with a $5\sigma_{FF}$ window. The number of molecules in the system and the corresponding point on the isotherm in Figure 4a are (top to bottom) 1325 − A, 2200 − B, 2225 − C, 2625 − D, and 2785 − E. Only molecules with centers located within a 1σ slice parallel to the plane of the picture are shown.

by the gauge cell.[26] At point D, the second pore fills, except for a bubble in it; such states are present until point E, where the bubble disappears. Line EF, where both pores are in the liquidlike state, does not differ from the corresponding part of the isotherm for a single pore.

The MCMC method allows one to construct a continuous function of $N(\mu)$, which can be thermodynamically integrated to determine the grand potential. The chemical potential at which VLE occurs can then be found, where the grand potentials of the filled pore and the pore with the adsorbed film are equal. We calculated the values of such equilibrium chemical potentials μ_e for each system by the application of Maxwell's rule of equal areas, applied to the grand potential[37]

$$\oint_{\mu_e} N(\mu)\, d\mu = 0 \tag{3}$$

Corresponding hypothetical VLE transitions are presented as vertical dashed lines in Figure 4. These calculations reveal that for the small window size ($5\sigma_{FF}$) the position of the equilibrium transition does not deviate substantially from that for the single sphere.

The adsorption branch of the GCMC isotherm for the two-pore model with the $5\sigma_{FF}$ window, presented in Figure 4a, almost coincides with the isotherm for a single pore; capillary condensation takes place at approximately the same chemical potential. However, the desorption branch of the GCMC isotherm has qualitatively different behavior than that for a single pore. The two-step desorption shows that the emptying of the neighboring pores in the two-pore model does not take place simultaneously, but the cavitation events are sequential. One of the desorption steps for the two-pore system in Figure 4a coincides with the desorption transition for a single pore. Intermediate states between two cavitation events correspond to the quasi-equilibrium states on the CD branch of the MCMC isotherm. Overall, because for a two-pore system with a small window we observe small deviations in equilibrium, condensation, and cavitation pressures, one should expect that the experimental behavior of the pore network with small windows should be similar to that in the system of independent spherical pores.

The MCMC isotherm for the two-pore system with the large window ($10\sigma_{FF}$) is presented in Figure 4b, and the snapshots for selected points on this isotherm are given in Figure 6. The MCMC isotherm has an intermediate loop; however, this loop is much less pronounced than that for the $5\sigma_{FF}$ window. Therefore, the range of chemical potential corresponding to quasi-equilibrium states, when the fluid in one of the pores is in the liquidlike state and the other remains in the vaporlike state (line CD), is narrower than for the system with a small window. For the system with a large window, a meniscus on the window between the pores in the CD region is revealed in the snapshots (snapshots for points C and C_1 in Figure 6). The proximity of the limit of stability of these states (point C) to the condition of equilibrium in the one-pore system (dotted line in Figure 4b) suggests that desorption from the partially saturated state may occur near the equilibrium. This scenario was first reported in ref 17 as an explanation of the substeps in the experimental scanning desorption isotherms.

Snapshots for points C and C_1, D_1 and D_2 are presented in Figure 6 to reveal an interesting "flip-flop" behavior, when the pore in the vapor state changes with the pore in the liquid state (C and C_1) or the bubble "moves" from one pore to another (D_1 and D_2). Apparently, because the pores are equivalent, such a flip-flop is not reflected in the thermodynamic state of the system.

Both the capillary condensation and cavitation transitions predicted by the GCMC isotherm for the two-pore model with the $10\sigma_{FF}$ window (Figure 4b) are shifted to higher chemical potentials, relative to the isotherm for a single pore. The hypothetical equilibrium VLE transition, calculated from the MCMC isotherm using the Maxwell rule (eq 3) is represented by the dashed line, which is also shifted to higher chemical potentials. These observations suggest that the experimental behavior of the pore network with large windows might deviate from that in the system of independent pores.

Another set of GCMC simulations was performed to test the stability of the quasi-equilibrium states branch (CDE in Figure 4) on the canonical ensemble MCMC isotherm.[38] In a single-pore model, any states between the vapor and liquid spinodal

dx.doi.org/10.1021/la302318j | Langmuir 2012, 28, 12100−12107

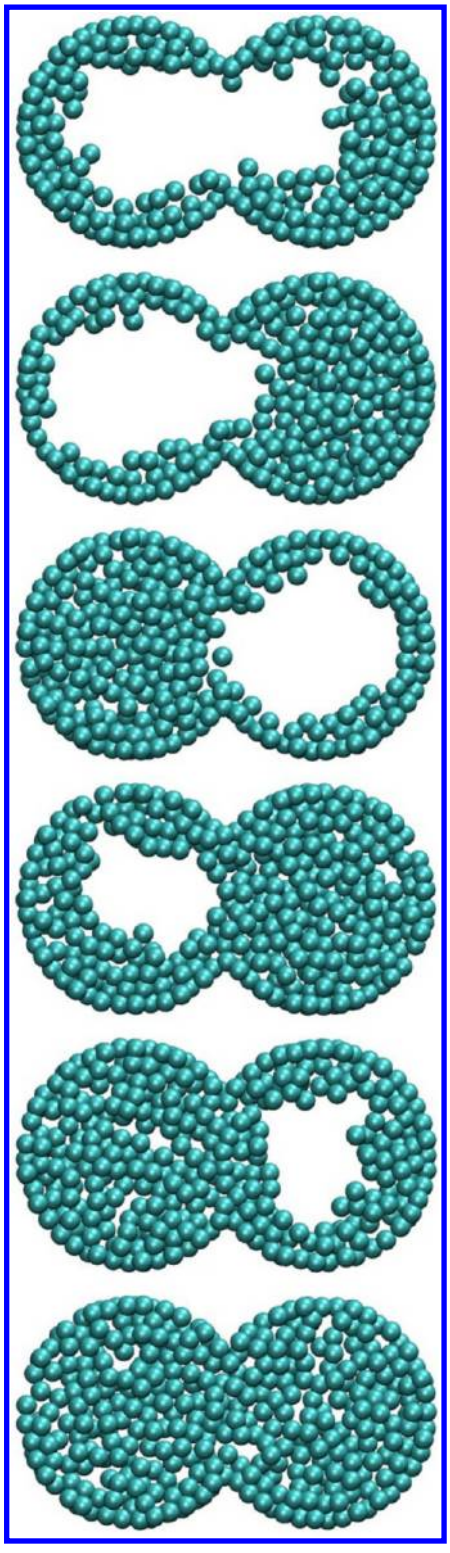

Figure 6. Snapshots of the molecules adsorbing in a system of two spheres with a $10\sigma_{FF}$ window. The number of molecules in the system and the corresponding points in Figure 4b are 2150 − B, 2200 − C, 2275 − C_1, 2625 − D_1, 2650 − D_2, and 2705 − E. Only molecules with centers located within a 1σ slice parallel to the plane of the picture are shown.

points (B and E, respectively) are known to be labile states and exist in the canonical ensemble on a single backward trajectory between the two points (i.e., the chemical potential on this trajectory decreases with the increase in the number of molecules). However, the canonical isotherm of the two-pore model presents three branches between the spinodals, two backward (BC and DE) and one forward (CE). To test the stability of these intermediate states, we take canonical ensemble configurations and set them in an open system as starting configurations for GCMC simulations by removing the gauge cell and fixing the chemical potential to the value of the previous simulation. The results of this study are presented in Figure 7. We found a significant range of stable one-sphere

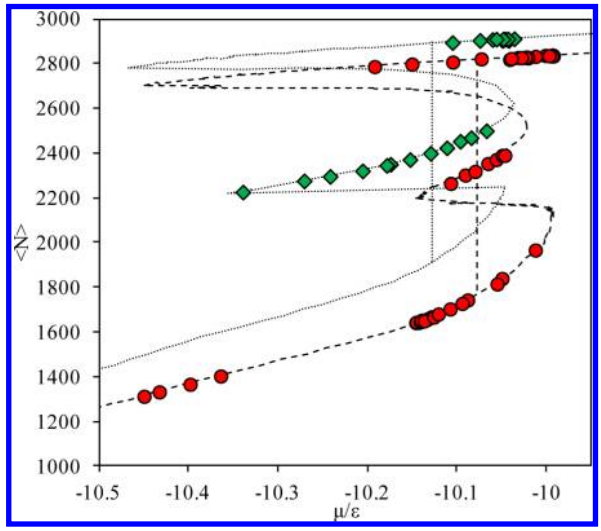

Figure 7. Stable states in GCMC simulation. The bold dashed line is the MCMC canonical isotherm for the $10\sigma_{FF}$ window, and the fine dashed line is for the $5\sigma_{FF}$ window. Circles and diamonds ($10\sigma_{FF}$ and $5\sigma_{FF}$, respectively) represent the $\langle N \rangle$ from a GCMC run using configurations from MCMC simulations as the initial state.

filled states (e.g., points C and C_1) for both $10\sigma_{FF}$ and $5\sigma_{FF}$ systems on the CD forward-trajectory branch. Any system starting on the DE backward-trajectory branch was found to be unstable because density fluctuations pushed the system to either a liquidlike or a vaporlike state. There were no states observed on the MCMC isotherms between points B and C. This confirms that the states when the fluid in one of the pores is in a liquidlike state and in the other is in a vaporlike state (i.e., a filled sphere in contact with an empty sphere via a meniscus) can be stable and further suggests the possibility of stepwise adsorption and desorption in such systems. It is important to note that although these intermediate states may be stable, that does not necessarily mean that they will be observed in experiments. The incremental increase in external pressure during adsorption measurements (and the corresponding decrease during desorption) would not permit access to the mid-density region that we observe during simulation. However, careful scanning isotherms could hypothetically probe this region.

Finally, to demonstrate the difference between desorption in the system with a 5σ window and the system with a 10σ window, we ran another series of GCMC simulations. We calculated the scanning desorption isotherms starting from the points obtained by MCMC within the CD region (Figure 4). The stability of these points was revealed above; now we test the limits of stability. Starting from a configuration when the fluid in one pore is in the liquid state and that in the other is in the vapor state and by sequentially decreasing the chemical

dx.doi.org/10.1021/la302318j | *Langmuir* 2012, 28, 12100−12107

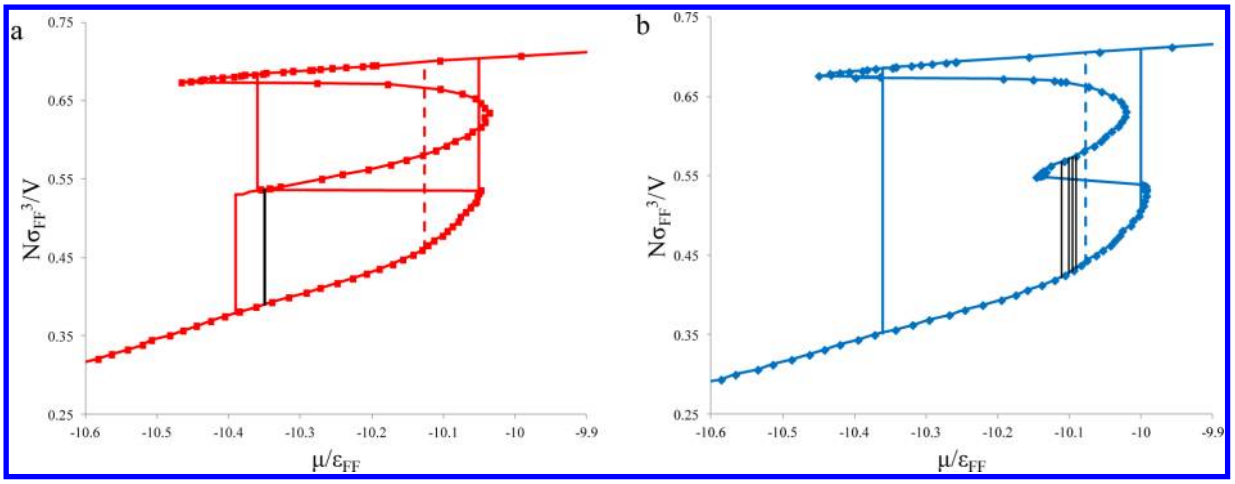

Figure 8. Scanning desorption isotherms for (a) a $5\sigma_{FF}$ window and (b) a $10\sigma_{FF}$ window. Scanning desorption isotherms are displayed with solid black lines connecting branches of corresponding gauge cell isotherms. Starting from a configuration when the fluid in one pore is in the liquid state and in the other is in the vapor state and by sequentially decreasing the chemical potential, we monitor the chemical potential at which evaporation takes place in the filled pore. Results for several runs are presented. Emptying of the filled pore in the system with a $10\sigma_{FF}$ window takes place at a substantially higher chemical potential than in the system with a $5\sigma_{FF}$ window.

potential, we monitor when the evaporation takes place in the filled pore. Results are presented in Figure 8, and scanning desorption isotherms are displayed with solid black lines connecting branches of corresponding MCMC isotherms. Thus, for the system with a 5σ window, the emptying of the filled pore takes place close to the liquid−vapor spinodal whereas for the system with a 10σ window we should expect evaporation at a substantially higher chemical potential, close to the equilibrium value for the single spherical pore. This confirms that pores with large windows should evaporate during the experiment at higher pressures than pores with small windows.

4. CONCLUSIONS

The adsorption and desorption of a Lennard-Jones fluid in the system of two overlapping spherical pores was modeled using mesocanonical and grand canonical Monte Carlo simulations. The system under consideration differed from the classical ink-bottle pore model in that it did not have connecting channels, which provide additional adsorption capacity. To reveal the role of the window size between the pores, we ran simulations for pores of the same diameter but with two different window sizes. This was compared with published results of simulations for the single spherical pore of the same diameter and adsorption potential. For the system with the small window, the values of the chemical potential at capillary condensation and evaporation predicted by GCMC simulations almost coincide with that of the single sphere of the same size. For the system with the large window, the positions of both capillary condensation and evaporation are noticeably shifted to higher values, reflecting the reduction of confinement effects.

Mesocanonical simulations allowed for trajectories of metastable and unstable states in the systems under consideration. In particular, we revealed points that correspond to the limit of stability of metastable configurations, when the fluid in one pore is in the liquid state and that in the other is in the vapor state with the meniscus at the window. For the system with the small window, the chemical potential of such a configuration is close to that of the liquidlike spinodal obtained in GCMC calculations. This implies that the vapor pressure at which capillary evaporation takes place in a system of overlapping spherical pores is close to the characteristic pressure of a single spherical pore, given a small degree of overlap.

For the system with the large window, the limit of stability of one-pore-filled configurations corresponds to a chemical potential that is substantially higher than that of the liquid−vapor spinodal and closer to the true vapor−liquid equilibrium determined by the Maxwell rule. This observation suggests that in a partially filled pore network with a relatively large overlap of pores, the evaporation along a scanning desorption isotherm may proceed at least partially in a near-equilibrium fashion. This conclusion complies with the earlier experimental studies of scanning desorption isotherms in FDU-1 materials with cagelike pore networks.[8]

The substantial difference between the mechanism of emptying the system with the small window and the mechanism of emptying the system with the large window was also revealed by simulating scanning desorption isotherms. Simulations of desorption starting from stable mid-density states revealed that pores with a small window empty close to the vapor−liquid spinodal whereas pores with a large window empty at a higher chemical potential close to the equilibrium value of the single spherical pore.

Overall, we can make an analogy between the considered model and the classical ink-bottle pore: for both models, the capillary condensation pressure is determined by the diameter of the main cavity, but the mechanism of desorption is controlled by the diameter of the necks/windows. The results can be used to understand the desorption mechanism in ordered materials with cagelike pores[22,25] or in some disordered materials.[5,39,40] The presented model of interconnected pores can be implemented for DFT calculations of adsorption/desorption isotherms to make a kernel for material characterization.

■ AUTHOR INFORMATION

Corresponding Author

*E-mail: aneimark@rutgers.edu.

Present Address

[†]Department of Civil and Environmental Engineering, Princeton University, E228 Engineering Quadrangle, Princeton, New Jersey 08544. E-mail: ggor@princeton.edu.

Notes

The authors declare no competing financial interest.

■ ACKNOWLEDGMENTS

We thank Matthias Thommes for fruitful discussions. This work was supported in part by the NSF ERC on structural organic composite systems, Quantachrome Instruments, and a Venkatarama Fellowship to C.J.R.

■ REFERENCES

(1) Neimark, A. V.; Ravikovitch, P. I. Capillary condensation in MMS and pore structure characterization. *Microporous Mesoporous Mater.* **2001**, *44*−*45*, 697−707.

(2) Ravikovitch, P. I.; Neimark, A. V. Calculations of Pore Size Distributions in Nanoporous Materials from Adsorption and Desorption Isotherms. In *Studies in Surface Science and Catalysis*; Nanoporous Materials II: Proceedings of the 2nd Conference on Access in Nanoporous Materials, Banff, Alberta, Canada, May 25−30, 2000; Sayari, A., Jaroniec, M., Pinnvaia, T. J., Eds.; Elsevier Science B. V.: Amsterdam, 2000; Vol. *129*, pp 597−606.

(3) Horikawa, T.; Do, D. D.; Nicholson, D. Capillary condensation of adsorbates in porous materials. *Adv. Colloid Interface Sci.* **2011**, *169*, 40−58.

(4) Monson, P. A. Understanding adsorption/desorption hysteresis for fluids in mesoporous materials using simple molecular models and classical density functional theory. *Microporous Mesoporous Mater.* **2012**, *160*, 47−66.

(5) Woo, H.-J.; Porcheron, F.; Monson, P. A. Modeling desorption of fluids from disordered mesoporous materials. *Langmuir* **2004**, *20*, 4743−4747.

(6) Nguyen, P. T. M.; Do, D. D.; Nicholson, D. On the cavitation and pore blocking in cylindrical pores with simple connectivity. *J. Phys. Chem. B* **2011**, *115*, 12160−12172.

(7) Edison, J. R.; Monson, P. A. Dynamic mean field theory of condensation and evaporation in model pore networks with variations in pore size. *Microporous Mesoporous Mater.* **2012**, *154*, 7−15.

(8) Coasne, B.; Galarneau, A.; Di Renzo, F.; Pellenq, R. J. M. Effect of morphological defects on gas adsorption in nanoporous silicas. *J. Phys. Chem. C* **2007**, *111*, 15759−15770.

(9) Gommes, C. J. Adsorption, capillary bridge formation, and cavitation in SBA-15 corrugated mesopores: a Derjaguin−Broekhoff−de Boer Analysis. *Langmuir* **2012**, *28*, 5101−5115.

(10) Zhao, D.; Feng, J.; Huo, Q.; Melosh, N.; Fredrickson, G. H.; Chmelka, B. F.; Stucky, G. D. Triblock copolymer syntheses of mesoporous silica with periodic 50 to 300 angstrom pores. *Science* **1998**, *279*, 548.

(11) Kleitz, F.; Czuryszkiewicz, T.; Solovyov, L. A.; Linden, M. X-ray structural modeling and gas adsorption analysis of cagelike SBA-16 silica mesophases prepared in a F127/butanol/H_2O System. *Chem. Mater.* **2006**, *18*, 5070−5079.

(12) McBain, J. W. An explanation of hysteresis in the hydration and dehydration of gels. *J. Am. Chem. Soc.* **1935**, *57*, 699−700.

(13) Thommes, M.; Smarsly, B.; Groenewolt, M.; Ravikovitch, P. I.; Neimark, A. V. Adsorption hysteresis of nitrogen and argon in pore networks and characterization of novel micro- and mesoporous silicas. *Langmuir* **2006**, *22*, 756−764.

(14) Rasmussen, C. J.; Vishnyakov, A.; Thommes, M.; Smarsly, B. M.; Kleitz, F.; Neimark, A. V. Cavitation in metastable liquid nitrogen confined to nanoscale pores. *Langmuir* **2010**, *26*, 10147−10157.

(15) Ravikovitch, P. I.; Neimark, A. V. Density functional theory of adsorption in spherical cavities and pore size characterization of templated nanoporous silicas with cubic and three-dimensional hexagonal structures. *Langmuir* **2002**, *18*, 1550−1560.

(16) Gregg, S. J.; Sing, K. S. W. *Adsorption, Surface Area, and Porosity*; Academic Press: New York, 1982.

(17) Ravikovitch, P. I.; Neimark, A. V. Experimental confirmation of different mechanisms of evaporation from ink-bottle type pores: equilibrium, pore blocking, and cavitation. *Langmuir* **2002**, *18*, 9830−9837.

(18) Sarkisov, L.; Monson, P. A. Modeling of adsorption and desorption in pores of simple geometry using molecular dynamics. *Langmuir* **2001**, *17*, 7600−7604.

(19) Vishnyakov, A.; Neimark, A. V. Monte Carlo simulation test of pore blocking effects. *Langmuir* **2003**, *19*, 3240−3247.

(20) Matos, J. R.; Kruk, M.; Mercuri, L. P.; Jaroniec, M.; Zhao, L.; Kamiyama, T.; Terasaki, O.; Pinnavaia, T. J.; Liu, Y. Ordered mesoporous silica with large cage-like pores: structural identification and pore connectivity design by controlling the synthesis temperature and time. *J. Am. Chem. Soc.* **2002**, *125*, 821−829.

(21) Sakamoto, Y.; Kaneda, M.; Terasaki, O.; Zhao, D. Y.; Kim, J. M.; Stucky, G.; Shin, H. J.; Ryoo, R. Direct imaging of the pores and cages of three-dimensional mesoporous materials. *Nature* **2000**, *408*, 449−453.

(22) Fan, W.; Snyder, M. A.; Kumar, S.; Lee, P.-S.; Yoo, W. C.; McCormick, A. V.; Lee Penn, R.; Stein, A.; Tsapatsis, M. Hierarchical nanofabrication of microporous crystals with ordered mesoporosity. *Nat. Mater.* **2008**, *7*, 984−991.

(23) Gor, G. Y.; Thommes, M.; Cychosz, K. A.; Neimark, A. V. Quenched solid density functional theory method for characterization of mesoporous carbons by nitrogen adsorption. *Carbon* **2012**, *50*, 1583−1590.

(24) Cychosz, K. A.; Guo, X.; Fan, W.; Cimino, R.; Gor, G. Y.;Tsapatsis, M.; Neimark, A. V.; Thommes, M. Characterization of the pore structure of three-dimensionally ordered mesoporous carbons using high resolution gas sorption. *Langmuir* **2012**, doi: la302362h.

(25) Wilke, A.; Weber, J. Mesoporous polymer networks−ultra-porous DVB resins by hard-templating of close-packed silica spheres. *Macromol. Rapid Commun.* **2012**, *33*, 785−790.

(26) Norman, G. E.; Filinov, V. S. Investigation of phase transitions by the Monte Carlo method. *High Temp. (USSR)* **1969**, *7*, 216−222.

(27) Neimark, A. V.; Vishnyakov, A. Gauge cell method for simulation studies of phase transitions in confined systems. *Phys. Rev. E* **2000**, *62*, 4611.

(28) Neimark, A. V.; Vishnyakov, A. A simulation method for the calculation of chemical potentials in small, inhomogeneous, and dense systems. *J. Chem. Phys.* **2005**, *122*, 234108−234111.

(29) Ravikovitch, P. I.; Vishnyakov, A.; Russo, R.; Neimark, A. V. Unified approach to pore size characterization of microporous carbonaceous materials from N-2, Ar, and CO_2 adsorption isotherms. *Langmuir* **2000**, *16*, 2311−2320.

(30) Baksh, M. S. A.; Yang, R. T. Model For spherical cavity radii and potential functions of sorbates in zeolites. *AIChE J.* **1991**, *37*, 923−930.

(31) Neimark, A. V.; Ravikovitch, P. I.; Grün, M.; Schüth, F.; Unger, K. K. Pore size analysis of MCM-41 type adsorbents by means of nitrogen and argon adsorption. *J. Colloid Interface Sci.* **1998**, *207*, 159−169.

(32) Neimark, A. V.; Vishnyakov, A. The birth of a bubble: a molecular simulation study. *J. Chem. Phys.* **2005**, *122*, 054707.

(33) Neimark, A. V.; Ravikovitch, P. I.; Vishnyakov, A. Inside the hysteresis loop: multiplicity of internal states in confined fluids. *Phys. Rev. E* **2002**, *65*, 031505.

(34) Vishnyakov, A.; Neimark, A. V. Multicomponent gauge cell method. *J. Chem. Phys.* **2009**, *130*, 224103−224109.

(35) Rasmussen, C. J.; Vishnyakov, A.; Neimark, A. V. Monte Carlo simulation of polymer adsorption. *Adsorption* **2011**, *17*, 265−271.

(36) Rasmussen, C. J.; Vishnyakov, A.; Neimark, A. V. Calculation of chemical potentials of chain molecules by the incremental gauge cell method. *J. Chem. Phys.* **2011**, *135*, 214109.

(37) Vishnyakov, A.; Neimark, A. V. Studies of liquid-vapor equilibria, criticality, and spinodal transitions in nanopores by the

gauge cell Monte Carlo simulation method. *J. Phys. Chem. B* **2001**, *105*, 7009−7020.
(38) Liu, Z.; Herrera, L.; Nguyen, V. T.; Do, D. D.; Nicholson, D.; Monte, A Carlo scheme based on mid-density in a hysteresis loop to determine equilibrium phase transition. *Mol. Simul.* **2011**, *37*, 932−939.
(39) Gelb, L. D. Modeling amorphous porous materials and confined fluids. *MRS Bull.* **2009**, *34*, 592−601.
(40) Casanova, F.; Chiang, C. E.; Ruminski, A. M.; Sailor, M. J.; Schuller, I. K. Controlling the role of nanopore morphology in capillary condensation. *Langmuir* **2012**, *28*, 6832−6838.